Platinum(II)–dithiocarbamate complexes with phosphines: Synthesis, characterization and precursor for Pt nanoparticles using ultrasound assisted method

Mawahib Q. Al-Douri[a*], *Asra'a* I. Yaseen [b], *Modher* Y. Mohammed [c]

Department of Chemistry, College of Education for Women, Tikrit University, Tikrit, Iraq

mawahibqsalih@gmail.com, asraay@gmail.com, modherymohammed@tu.edu.iq

Abstract. The reaction between $Na_2[PtCl_4]$ and thymine bis-dithiocarbamate (tdtc) in a 2:1 molar ratio (Metal:Ligand) produced a square planar complex called $[Pt(tdtc)_2]_n$ (1). By reacting $[Pt(tdtc)_2]_n$ with different phosphine ligands, such as $Ph_2PCH_2PPh_2$ (dppm), $Ph_2PCH_2CH_2CH_2PPh_2$ (dppp), and PPh_3, the complexes $[Pt(dtc)_2(dppm)_2]_n$, $[Pt(dtc)_2(dppp)]_n$ and $[Pt(tdtc)_2(PPh_3)_2]_n$ were obtained. Various characterization techniques, including FTIR, molar conductivity, ^{1}H-NMR, and ^{31}P-NMR, were used to analyze these complexes. The results demonstrated that the tdtc ligand acts as a monodentate ligand, binding to the metal center through the soft sulfur atom in the presence of phosphines and bidentate chelating in the absence of phosphines. Furthermore, the complex $[Pt(dtc)_2(dppp)]_n$ was transformed into platinum nanoparticles (Pt NPs) through the application of ultrasound. The resulting platinum nanoparticles were characterized using UV-Vis, TEM, and XRD.

Keywords: Platinum complexes, dithiocarbamate, thymine, platinum nanoparticles

1. Introduction

Coordination compounds with ligands containing heteroatoms are still the most important compounds for different applications [1-5]. Dithiocarbamate complexes, a class of coordination compounds, have garnered significant attention due to their diverse applications in various fields of science and technology. These complexes exhibit fascinating properties, making them valuable in areas such as catalysis, medicinal chemistry, materials science, and environmental sciences. One of the distinguishing features of dithiocarbamate complexes is the presence of a sulfur-containing ligand, which plays a crucial role in their reactivity and functionality. Dithiocarbamates, represented by the formula $RR'NCS^{2-}$, have long captured the interest of coordination chemists due to their remarkable versatility [6-10]. These ligands, typically monovalent anionic species, exhibit a symmetrical coordination pattern through their two sulfur atoms, forming stable complexes

*mawahibqsalih@gmail.com**

with a diverse range of metals in various oxidation states, often surpassing the typical coordination preferences. However, it is worth mentioning that bridging coordination modes have been occasionally observed in the structural chemistry of main group elements [11-14]. While rare, polyfunctional dithiocarbamate ligands, featuring multiple CS^{2-} units, have been reported [15]. Additionally, ligands with both CS^{2-} functionality and other coordinating sites, such as pyridyl donors, exist, leading to bridging multi-metallic aggregates [16]. The structural diversity of dithiocarbamate complexes is a subject of considerable interest due to their ability to coordinate with a wide variety of heavy metal ions, leading to the formation of diverse and intriguing structural motifs. In the realm of platinum dithiocarbamates, binary structures are predominantly observed, as evidenced by X-ray crystallography studies. These structures predominantly exhibit square planar geometries, where the coordination is facilitated by two chelating dithiocarbamate ligands, providing a donor set comprising four sulfur atoms (S_4). This motif is consistently observed in the previously characterized complexes [17-19], with a few exceptions. Notably, the introduction of phosphine ligands alters the coordination geometry around platinum, leading to a modified geometry characterized by a combination of two sulfur atoms and two phosphine atoms (S_2P_2) [20]. Dithiocarbamate-containing complexes have been widely employed as single source precursors (SSP) in the synthesis of nanomaterials featuring a central metal because of that the dithiocarbamate ligand acts as capping agent and the complex as metal source [21]. These complexes have shown a tendency to yield nanoscale metal sulfides when the reaction is conducted under an inert gas atmosphere, such as nitrogen [22]. The interaction between the dithiocarbamate ligands and the metal precursor results in the formation of sulfide nanoparticles. This process is typically driven by the thermal decomposition of the dithiocarbamate ligands, leading to the sulfur atoms coordinating with the metal ions and facilitating the formation of metal sulfides.

However, it is noteworthy that alternative methods involving oxidation at elevated temperatures have been explored, leading to the production of other components rather than metal sulfides. In these cases, the high temperatures induce the oxidation of the metal precursor, resulting in the formation of the corresponding metal oxides [23, 24]. The transformation from metal sulfides to metal oxides can be attributed to the thermal stability and reactivity of the dithiocarbamate ligands under such conditions.

These alternative synthetic strategies offer new avenues for tailoring the composition and properties of the nanocomposites. By adjusting the reaction conditions and introducing oxidation steps, it becomes possible to modulate the composition of the final nanomaterials, thereby expanding their potential applications. The precise control over the composition and structure of the nanocomposites opens up opportunities for exploring their unique physicochemical properties and harnessing them for various technological applications. This work includes the preparation of new complexes of platinum with dithiocarbamates and mono- and bi-dentate phosphines and the study of their coordination chemistry. Furthermore, an experiment was made to prepare platinum nanoparticles from one of the complexes which act as an SSP and then diagnose it using TEM and XRD.

2. Experimental

2.1. Chemicals and instruments

Sodium tetrachloropalatinate, carbon disulfide, thymine and sodium hydroxide were purchased from Sigma-Aldrich.

The Bruker 400 NMR spectrometer was used to record ^{1}H- and ^{31}P-NMR spectra. The measurements were performed in DMSO-d6 as the solvent. The SHIMADZU FTIR-8400S spectrophotometer was employed to record FTIR spectra. The spectra were obtained using

KBr discs in the range of 400–4000 cm^{-1}. The Stuarts SMP10 melting point apparatus was utilized to measure the melting point. The apparatus has an error range of ±3 ºC. The Eager 300 for EA1112 instrument was used for CHN analysis, providing elemental composition information. Zeiss TEM and Shimadzu XRD devices were used to characterize the Pt nanoparticles.

2.2. Synthesis

2.2.1. Thyminebis(dithiocarbamate) (TDTC)

A total of 0.928 g (15.85 mmol) of carbon disulfide (CS_2) was added to a solution of 1 g (7.92 mmol) of thymine in 15 ml of hot distilled water. To facilitate the reaction, 0.634 g (15.85 mmol) of NaOH was included in the mixture. The resulting solution was stirred for three hours using an ice bath to maintain a temperature range of 0 to 7 ºC. Throughout the stirring process, the solution gradually transformed into a light orange-colored solution.

After completion of the reaction, the mixture was filtered to remove any insoluble impurities. The filtrate was then subjected to evaporation in a water bath set at 50 ºC for pre-drying purposes. Subsequently, the precipitate formed during evaporation was carefully collected. Finally, the collected precipitate was dried in an electric oven at a temperature of 50 ºC for a duration of ten hours to obtain the ligand in its final form.
The reaction is shown in the following equation:

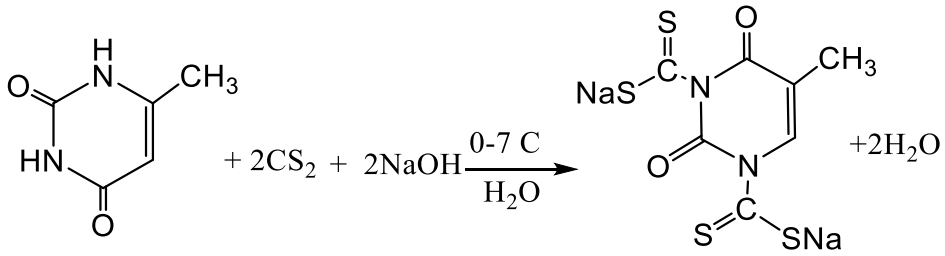

The ligand tdtc: Orange solid, 92 %. Anal. Calc. for $C_7H_4N_2Na_2O_2S_4$: C, 26.08; H, 1.25; N, 8.69 Found: C, 26.08; H, 1.25; N, 8.69 %. IR (KBr, cm^{-1}): 1627 (C=O), 1512 (C=O), 1480 (C=C), 1458 (C=C), 1388 (C=N), 1053 (C=S), 860 (C-S).^{1}H-NMR (DMSO-*d6*, δ ppm):7.25 (s, 1H, tdtc), 1.72 (s, 3H, tdtc). M.p (ºC): 300 decomposition.

2.2.2. $[Pt(tdc)_2]_n$ (1)

The ligand tdtc (0.5 g, 1.551 mmol) was dissolved in 15 ml of distilled water, and this solution was added to a separate solution of Na_2PtCl_4 (1.28 g, 3.102 mmol) in 15 ml of distilled water. Upon addition, an instant formation of a dark orange solution occurred. The resulting mixture was stirred for a duration of three hours. Following the stirring period, the precipitate that formed was collected by filtration and subsequently washed with distilled water. The collected precipitate was then dried in an electric oven at a temperature of 50 ºC for three hours. The overall yield of the process was 82%.
Deep brown solid, 88 %. Anal. Calc. for $C_{14}H_8N_4O_4PtS_8$: C, 22.49; H, 1.08; N, 7.49, Found: C, 22.55; H, 1.11; N, 7.50%. A_M= 25.5 cm^{-1} Ohm^{-1} mol^{-1}. IR (KBr, cm^{-1}):1693 (C=O), 1000 (C=S). ^{1}H-NMR (DMSO-*d6*, δ ppm):7.70 (s, 1H, tdtc), .190 (s, 3H, tdtc). M.p (ºC): 250-252.

2.2.3. $[Pt(tdtc)_2(PPh_3)_2]_n$ (2)

A solution of PPh_3 (0.0647 g, 0.246 mmol) in 10 ml of acetone was combined with a solution of $[Pt(tdtc)_2]_n$ (0.05 g, 0.0617 mmol) in 10 ml of distilled water. The resulting mixture was stirred for a period of two hours, resulting in the formation of a gray precipitate. The precipitate was separated by filtration and subsequently washed with distilled water. Afterward, the collected precipitate was dried in an electric oven at a temperature of 50 ºC for 7 hours.
Gray solid, 55%. Anal. Calc. for $C_{50}H_{38}N_4O_4P_2PtS_8$: C, 47.20; H, 3.01; N, 4.40, Found: C, 47.220; H, 3.08; N, 4.40%. A_M= 27.5 cm^{-1} Ohm^{-1} mol^{-1}. IR (KBr, cm^{-1}): 1670 (C=O), 1431 (P-Ph), 1022 (C-S), 944 (C-S), ^{1}H-NMR (DMSO-*d6*, δ ppm): 7.52 (s, 2H, 2tdtc), .162 (s, 6H, 2tdtc), 7.2 - 7.5 (broad, 20H, $2PPh_3$). M.p (ºC): 228-230.
The method in 2.2.3 was used to prepare other phosphine complexes **$[Pt(tdtc)_2(dppm)_2]_n$ (3)** and **$[Pt(tdtc)_2(dppp)]_n$ (4)**.
$[Pt(tdtc)_2(dppm)_2]_n$ (3): Dark olive solid, 61%. Anal. Calc. for $C_{64}H_{52}N_4O_4P_4PtS_8$: C, 50.69; H, 3.46; N, 3.69, Found: C, 50.73; H, 3.50; N, 3.70%. A_M= 14.5 cm^{-1} Ohm^{-1} mol^{-1}. IR (KBr, cm^{-1}): 1674 (C=O), 1433 (P-Ph), 1029 (C-S), 949 (C-S), ^{1}H-NMR (DMSO-*d6*, δ ppm): 7.81 (s, 2H, 2tdtc), 1.74 (s, 6H, 2tdtc), 7.26 -7.50 (broad, 40H, 2dppm), 2.99 (s, 4H, 2dppm). M.p (ºC): 190-194.
$[Pt(tdtc)_2(dppp)]_n$ (4): Dark brown solid, 94%. Anal. Calc. for $C_{41}H_{34}N_4O_4P_2PtS_8$: C, 42.44; H, 2.95; N, 4.83, Found: C, 42.86; H, 2.99; N, 4.91%. A_M= 20.5 cm^{-1} Ohm^{-1} mol^{-1}. IR (KBr, cm^{-1}): 1654 (C=O), 1431 (P-Ph), 1022 (C-S), 991 (C-S), ^{1}H-NMR (DMSO-*d6*, δ ppm): 7.03 (s, 2H, 2tdtc), 1.74 (s, 6H, 2tdtc), 7.52 – 8.08 (broad, 20H, dppp), 1.82 (s, 2H, dppp), 1.30 (virtual t, 4H, dppp). M.p (ºC): 243-246.

2.2.4. Pt nanoparticles

The complex $[Pt_2(tdtc)_2(dppp)_2Cl_2]$ was used as a starting material for the preparation of Pt nanoparticles. 1 g of the complex $[Pt_2(tdtc)_2(dppp)_2Cl_2]$ was added to 75 ml of deionized water and stirred for 10 minutes at room temperature on a magnetic stirrer at a speed of 350 rpm. Thereafter, the solution sonicated using ultrasound with 150 W for an hour until a reddish-black precipitate was formed. The product was isolated by centrifuge the mixture at a speed of 11500 rpm at a temperature of 10°C. The supernatant was collected for further using and stored at 5 ºC.

3. Results and discussion

3.1. Melting points and molar conductivity

The experimental findings confirmed the synthesis of novel compounds exhibiting distinct coloration compared to the starting materials, along with melting point values significantly divergent from those observed for the original ligand, surpassing the threshold of 300 °C. Conductivity measurements provided evidence that all the synthesized complexes were non-ionic in nature, with the highest recorded conductivity value reaching 27.5 cm^{-1} Ohm^{-1} mol^{-1}. This finding implies that the conductivity of these complexes is comparatively lower than that typically observed for ionic compounds [25, 26].

3.2. FTIR

3.2.1. FTIR of TDTC ligand

The prepared ligand (tdtc) was identified by studying its infrared spectrum and comparing it with the infrared spectrum of the raw material used in the preparation of the ligand [27, 28]. The disappearance of the absorption band at 3190 cm^{-1} corresponding to the ν (N-H) group in thymine serves as compelling evidence for the deprotonation of the amine group, resulting in the attachment of CS_2 to the nitrogen atom. Additionally, the spectrum exhibits bands at 2364 cm^{-1} and 2943 cm^{-1}, which can be attributed to the symmetrical and asymmetric stretching of the aliphatic ν(C-H) group [27-31]. Notably, sharp intensity bands at 1627 cm^{-1} and 1512 cm^{-1} indicate the stretching vibration of ν(C=O) in thymine, while bands at 1480 cm^{-1} and 1458 cm^{-1} are indicative of the symmetrical and asymmetric stretching of the (C=C) group, respectively, in thymine. The first distinctive band of the dithiocarbamate emerges at 1388 cm^{-1}, representing the partial double bond of (C=N), which lies between the single (C-N) and double (C=N) bonds. The second characteristic band manifests as two bands at 1053 cm^{-1} and 1114 cm^{-1} , attributable to the stretching vibrations of ν(C=S) [29]. Lastly, the third characteristic band appears at 860 cm^{-1}, signifying the bond (S-C).

3.2.2. FTIR spectra of the complexes

The FT-IR spectra of all complexes exhibited a prominent band in the range of 1674-1654 cm^{-1}, corresponding to the stretching vibration of ν(C=O), which coincided with the frequency observed for the tdtc ligand [31]. This observation suggests that there is no coordination to the metal center through oxygen sites in tdtc. The infrared spectra of the complexes also displayed absorption bands in the ranges of 948-995 cm^{-1} and 1022-1029 cm^{-1}, which can be attributed to the stretching vibrations of C=S and C-S, respectively. These bands were observed at lower frequencies compared to those observed for the free tdtc ligand. Notably, the presence of two distinct C=S bands indicates the coordination of both sulfur atoms to the metal ion, thus confirming a monodentate mode [32]. However, in the case of $[Pt(tdtc)_2]_n$, only one band was observed at 1000 cm^{-1}. Additionally, the complexes containing phosphine ligands displayed bands in the ranges of 1454-1431 cm^{-1} and 1091-1087 cm^{-1}, which can be attributed to the stretching vibrations of P-Ph [33].

3.3. ^{1}H-NMR spectra of the as-prepared ligand and complexes

3.3.1. ^{1}H-NMR spectrum of the tdtc ligand

The ^{1}H-NMR spectrum of the ligand (tdtc) showed only one singlet signal at the 1.72 ppm due to the protons of the (CH) group in thymine. The spectrum also showed singlet signal at the 7.25 ppm assigned to the protons of the CH-N group [34]. The absence or disappearance of NH signals further supports the formation of the dithiocarbamate moiety.

3.3.2. ^{1}H NMR spectrum of $[Pt(tdtc)_2]_n$ complex

The ^{1}H-NMR spectrum of the synthesized complex $[Pt(tdtc)_2]_n$ exhibited a singlet signal at 1.9 ppm, which can be attributed to the (CH_3) group, and a singlet signal at 7.7 ppm corresponding to the CH=N group [35].

3.3.3. ^{1}H NMR spectrum of complex $[Pt(tdtc)_2(PPh_3)_2]_n$

In the ^{1}H-NMR spectrum of $[Pt(tdtc)_2(PPh_3)_2]_n$, a singlet signal was observed at 1.64 ppm, corresponding to the CH_3 group of the tdtc ligand. Additionally, a singlet signal appeared at 7.52 ppm, representing the alkene proton of tdtc. Furthermore, a multiplet signal was observed in the range of 7.2 - 7.5 ppm, with an integration corresponding to 20 protons. The integration of these signals suggests their origin from the protons of the six aromatic rings present in the PPh_3 ligand. The integration of the tdtc and PPh_3 signals proves the presence of tdtc and PPh_3 in 1:1 ratio.

3.3.4. ^{1}H-NMR spectrum of a complex of $[Pt(tdtc)_2(dppm)_2]_n$

In the ^{1}H-NMR spectrum of $[Pt(tdtc)_2(dppm)_2]_n$, a singlet signal was observed at 1.74 ppm, corresponding to the CH_3 group of the tdtc ligand. Additionally, a singlet signal appeared at 7.81 ppm, representing the alkene proton of tdtc. Furthermore, a multiplet signal was observed in the range of 7.26 - 7.5 ppm, with an integration corresponding to 40 protons of dppm in addition to a singlet signal at 2.99 ppm of CH_2 in dppm. The integration of these signals suggests their origin from the protons of the 8 aromatic rings present in the dppm ligand. The integration of the tdtc and dppm signals proves the presence of 1:1 ratio.

3.3.5. ^{1}H-NMR spectrum of a complex of $[Pt(tdtc)_2(dppp)]_n$

In the ^{1}H-NMR spectrum of $[Pt(tdtc)_2(dppp)]_n$, a singlet signal was observed at 1.74 ppm, corresponding to the CH_3 group of the tdtc ligand. Additionally, a singlet signal appeared at 7.03 ppm, representing the alkene proton of tdtc. Furthermore, a multiplet signal was observed in the range of 7.52 – 8.08 ppm, with an integration corresponding to 20 protons of dppp in addition to a broad signal at 1.82 ppm of middle CH_2 in dppp in addition to virtual triplet at 1.30 ppm of terminal CH_2 groups. The integration of these signals suggests their origin from the protons of the 4 aromatic rings present in the dppp ligand. The integration of the tdtc and dppp signals proves the presence of 2:1 ratio, respectively.

3.4. ^{31}P-NMR spectrum

The ^{31}P-NMR spectrum of the complexes $[Pt(tdtc)_2(PPh_3)_2]_n$ and $[Pt(tdtc)_2(dppp)]_n$ showed a single signal at $\delta^{31}P$ = 25.57 and 30.01 ppm with satellite of *J* Pt-P=4000-4040 Hz, as the single signal indicates the presence of one compound in which the phosphorus atoms are equivalent and it is chelated. The complex $[Pt(tdtc)_2(dppm)_2]_n$ showed two doublet signals at 27.47 and -28.16 ppm, which prove the monodentate bound of dppm to Pt ion [36].

3.5. Characterization of Pt NPs

3.5.1. UV-Visible

The UV-Vis spectrum of Pt nanoparticles (Figure 1) exhibited a solitary intense peak at 250 nm, providing evidence for the formation of platinum nanoparticles. This peak, which is commonly observed at this wavelength [37], confirms the presence and characteristic behavior of platinum nanoparticles.

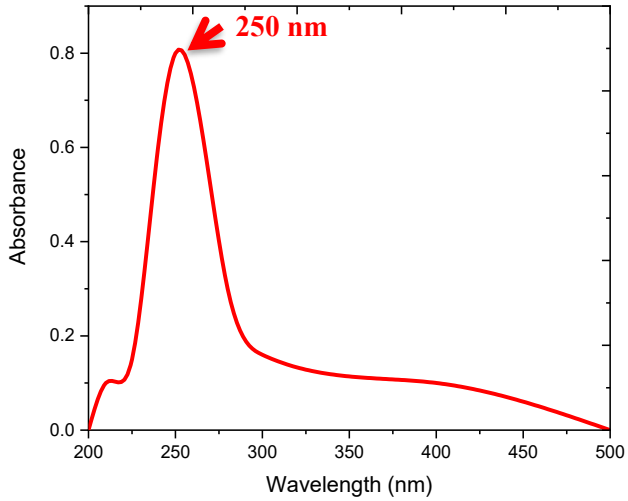

Fig. 1. UV-Vis of Pt NPs

3.5.2. TEM

The formation of platinum nanoparticles in the form of nanoassemblies was confirmed through TEM measurements (Figure 2), which revealed the presence of nanoparticles with sizes ranging up to 70 ± 20 nm. These nanoparticles exhibited a distinctive morphology, appearing as nanoballs formed by the aggregation of numerous smaller particles. This observation strongly suggests the formation of platinum nanoparticles in the form of nanoassemblies. Importantly, these findings are consistent with previous studies documented in the literature [37, 38].

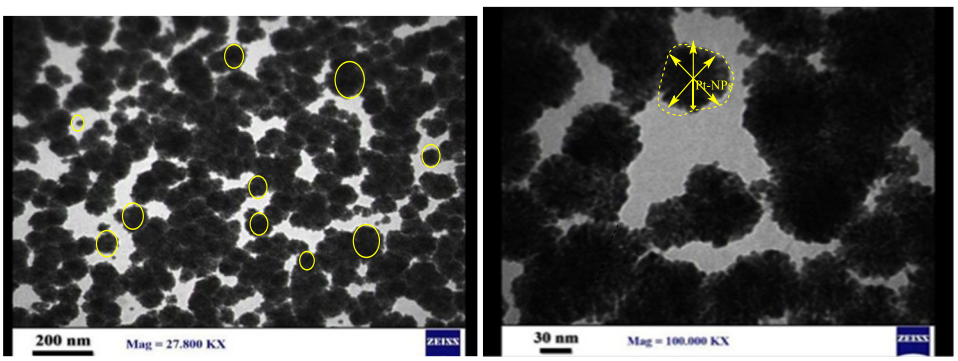

Fig. 2. TEM of Pt NPs with different magnifications

3.5.3. XRD of Pt NPs

The XRD measurement of the platinum nanoparticles (Figure 3) showed the main peaks at 40.085 (111), 45.4632 (200), 46.644 (102) and 68.07 (220) degree which are the characteristic peaks for platinum nanoparticles, as shown in Figure 2. However the other peaks could be attributed to the remnant of the ligands from the starting complex [37].

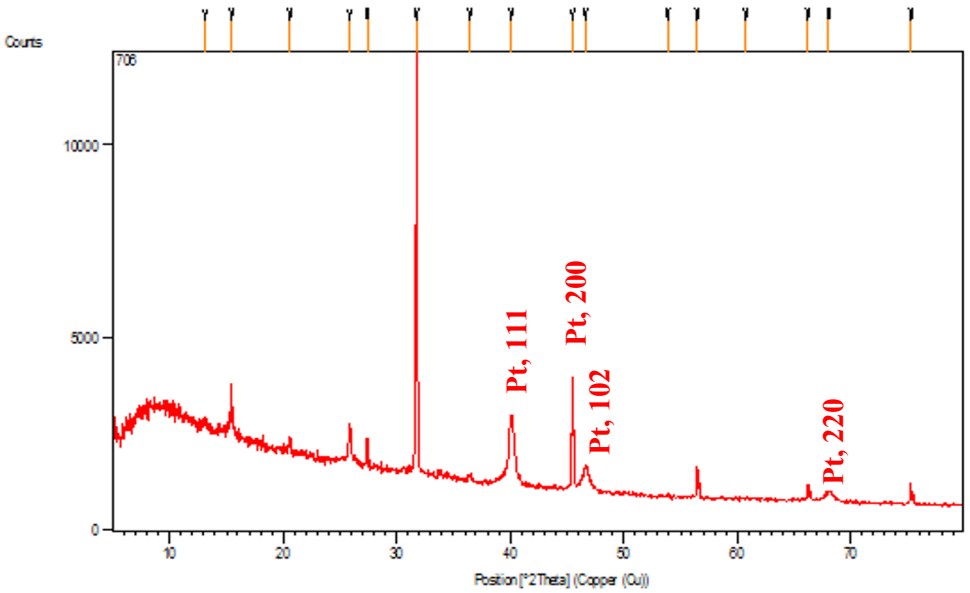

Fig. 3. XRD of Pt NPs

3.6. A comparative study

A comparative study in Table 1 was conducted to evaluate various synthesis methods for platinum nanoparticles. Previous approaches involved the utilization of two different raw materials, namely K_2PtCl_4 and H_2PtCl_6, as platinum sources [38-42]. However, these materials necessitated the inclusion of additional polymeric substances to facilitate the conversion into corresponding nanometal entities, thereby impeding nanoparticle aggregation and leading to the presence of extraneous components. Moreover, these methods yielded nanoparticles with a broad size distribution and fixed geometric shapes. In contrast, the current investigation represents a pioneering study by introducing a novel raw material and an environmentally benign manufacturing technique, namely ultrasound-assisted synthesis, obviating the requirement for dispersants. Consequently, this methodology can be regarded as a single source precursor (SSP) approach, enabling precise control over nanoparticle characteristics.

Table 1. Comparison study between Pt nps synthesis methods, shape, particle size and starting materials

Synthesis Method	Starting Material	Particle Size (nm)	Shape	Ref.
Chemical Reduction	K_2PtCl_4	12.9–70.7	Spherical	[44]
Sol-Gel Method	K_2PtCl_4	20-144	Spherical and cube	[45]
Electrochemical Deposition	H_2PtCl_6	40	Agglomerate from irregular particles	[46]
Green Synthesis	H_2PtCl_6	30–60	irregular	[47]
Ultrasound	$[Pt(tdtc)_2(dppp)]_n$	70 ± 20	Agglomerate from spherical particles	This study

4. Conclusion

We concluded that thymine bisdithiocarbamate ligand has the ability to coordinate bidentate chelating across both sulfur atoms of the dithiocarbamate group and monodentate in the presence of phosphines. In terms of nanotechnology, platinum nanoparticles were synthesized using $[Pt(tdtc)_2(dppp)]_n$ complex as a raw material. The results prove that platinum was prepared with nano sizes less than (80 nm) with regular nanostructures (nanoball). A platinum atom surrounded by many organic molecules, allows platinum to grow with more regular nanostructures than if salts were used directly.

References

1. Allawi, A. H., Alheety, M. A., & Mohammed, M. Y. (2022). Ultrasound assisted synthesis of attapulgite-PdO nanocomposite using palladium complex for hydrogen storage: Kinetic studies. *Inorganic Chemistry Communications*, *143*, 109787.
2. Alheety, M. A., Majeed, A. H., Ali, A. H., Mohammed, L. A., Destagul, A., & Singh, P. K. (2022). Synthesis and characterization of eggshell membrane polymer-TiO2 nanocomposite for newly synthesized ionic liquid release. *Journal of the Iranian Chemical Society*, *19*(9), 4005-4015.
3. Alheety, N. F., Mohammed, L. A., Majeed, A. H., Sehgal, S., Aldahham, B. J., & Alheety, M. A. (2022). The effect of addition Ag and MnO2 nanoparticles in the hydrogen storage of ethyl 2-((5-methoxybenzo [d] thiazol-2-yl) thio) acetate (organic: Inorganic nanohybrids). *Journal of the Indian Chemical Society*, *99*(10), 100734.
4. Alheety, N. F., Mohammed, L. A., Majeed, A. H., Sehgal, S., Aldahham, B. J., & Alheety, M. A. (2022). The effect of addition Ag and MnO2 nanoparticles in the hydrogen storage of ethyl 2-((5-methoxybenzo [d] thiazol-2-yl) thio) acetate (organic: Inorganic nanohybrids). *Journal of the Indian Chemical Society*, *99*(10), 100734.
5. Mohammed, L. A., Majeed, A. H., Hammoodi, O. G., Prakash, C., Alheety, M. A., Buddhi, D., ... & Mohammed, I. K. (2022). Design and characterization of novel ternary nanocomposite (rGO-MnO2-PoPDA) product and screening its dielectric properties. *International Journal on Interactive Design and Manufacturing (IJIDeM)*, 1-15.
6. Coucouvanis, D. The chemistry of the dithioacid and 1,1-dithiolate complexes. In *Progress in Inorganic Chemistry*; Lippard, S.J., Ed.; John Wiley & Sons: Hoboken, NJ, USA, 1970; Volume 11, pp. 234–371.
7. Eisenberg, R. Structural systematics of 1,1- and 1,2-dithiolato chelates. In *Progress in Inorganic Chemistry*; Lippard, S.J., Ed.; John Wiley & Sons: Hoboken, NJ, USA, 1970; Volume 12, pp. 295–369.
8. Coucouvanis, D. The chemistry of the dithioacid and 1,1-dithiolate complexes, 1968–1977. In *Progress in Inorganic Chemistry*; Lippard, S.J., Ed.; John Wiley & Sons: Hoboken, NJ, USA, 1979; Volume 26, pp. 301–469.
9. Hogarth, G. Transition metal dithiocarbamates: 1978–2003. In *Progress in Inorganic Chemistry*; Karlin, K.D., Ed.; John Wiley & Sons: Hoboken, NJ, USA, 2005; Volume 53, pp. 71–561.
10. Heard, P.J. Main group dithiocarbamate complexes. In *Progress in Inorganic Chemistry*; Karlin, K.D., Ed.; John Wiley & Sons: Hoboken, NJ, USA, 2005; Volume 53, pp. 1–69.
11. Tiekink, E.R.T. Aggregation patterns in the crystal structures of organometallic Group XV 1,1-dithiolates: The influence of the Lewis acidity of the central atom, metal- and

ligand-bound steric bulk, and coordination potential of the 1,1-dithiolate ligands upon supramolecular architecture. *CrystEngComm* **2006**, *8*, 104–118.

12. Tiekink, E.R.T.; Zukerman-Schpector, J. Stereochemical activity of lone pairs of electrons and supramolecular aggregation patterns based on secondary interactions involving tellurium in its 1,1-dithiolate structures. *Coord. Chem. Rev.* **2010**, *254*, 46–76.
13. Tiekink, E.R.T. Exploring the topological landscape exhibited by binary zinc-triad 1,1-dithiolates. *Crystals* **2018**, *8*, 292.
14. Tiekink, E.R.T. Perplexing coordination behaviour of potentially bridging bipyridyl-type ligands in the coordination chemistry of zinc and cadmium 1,1-dithiolate compounds. *Crystals* **2018**, *8*, 18.
15. Lee, S.M.; Tiekink, E.R.T. A structural survey of poly-functional dithiocarbamate ligands and the aggregation patterns they sustain. *Inorganics* **2021**, *9*, 7.
16. Tiekink, E.R.T. On the coordination role of pyridyl-nitrogen in the structural chemistry of pyridyl-substituted dithiocarbamate ligands. *Crystals* **2021**, *11*, 286.
17. Poirier, S.; Lynn, H.; Reber, C.; Tailleur, E.; Marchivie, M.; Guionneau, P.; Probert, M.R. Variation of M···H–C interactions in square-planar complexes of nickel(II), palladium(II), and platinum(II) probed by luminescence spectroscopy and X-ray diffraction at variable pressure. *Inorg. Chem.* **2018**, *57*, 7713–7723.
18. Poirier, S.; Guionneau, P.; Luneau, D.; Reber, C. Why do the luminescence maxima of isostructural palladium(II) and platinum(II) complexes shift in opposite directions? *Can. J. Chem.* **2014**, *92*, 958–965.
19. Ferreira, I.P.; de Lima, G.M.; Paniago, E.B.; Takahashi, J.A.; Pinheiro, C.B. Synthesis, characterization and antifungal activity of new dithiocarbamate-based complexes of Ni(II), Pd(II) and Pt(II). *Inorg. Chim. Acta* **2014**, *423*, 443–449.
20. Knight, E.R.; Leung, N.H.; Lin, Y.H.; Cowley, A.R.; Watkin, D.J.; Thompson, A.L.; Hogarth, G.; Wilton-Ely, J.D.E.T. Multimetallic arrays: Symmetrical bi-, tri- and tetrametallic complexes based on the group 10 metals and the functionalisation of gold nanoparticles with nickel-phosphine surface units. *Dalton Trans.* **2009**, 3688–3697.
21. Scott, J.A.; Angeloski, A.; Aharonovich, I.; Lobo, C.J.; McDonagh, A.; Toth, M. In situ study of the precursor conversion reactions during solventless synthesis of Co_9S_8, Ni_3S_2, Co and Ni nanowires. *Nanoscale* **2018**, *10*, 15669–15676.
22. Roffey, A.; Hollingsworth, N.; Islam, H.U.; Mercy, M.; Sankar, G.; Catlow, C.R.; Hogarth, G.; de Leeuw, N.H. Phase control during the synthesis of nickel sulfide nanoparticles from dithiocarbamate precursors. *Nanoscale* **2016**, *8*, 11067–11075.
23. Breviglieri, S.T.; Cavalheiro, É.T.G.; Chierice, G.O. Correlation between ionic radius and thermal decomposition of Fe(II), Co(II), Ni(II), Cu(II) and Zn(II) diethanoldithiocarbamates. *Thermochim. Acta* **2000**, *356*, 79–84.
24. Doherty, R. E., Sazanovich, I. V., McKenzie, L. K., Stasheuski, A. S., Coyle, R., Baggaley, E., ... & Bryant, H. E. (2016). Photodynamic killing of cancer cells by a Platinum (II) complex with cyclometallating ligand. *Scientific reports*, *6*(1), 1-9.
25. Francos, J., & Cadierno, V. (2019). The chemistry of guanidinate complexes of the platinum group metals. *Dalton Transactions*, *48*(25), 9021-9036.
26. Mohammad, E. T. (2018). University of Mosul.
27. Nakamoto, K., Fujita, J., Condrate, R. A., & Morimoto, Y. (1963). Infrared spectra of metal chelate compounds. IX. A normal coordinate analysis of dithiocarbamato complexes. *The Journal of Chemical Physics*, *39*(2), 423-427.

28. Beć, K. B., & Grabska, J. (2018). Quantum mechanical simulations of near-infrared spectra of biomolecules–Long-chain fatty acids. *NIR news*, *29*(6), 13-19.
29. Preti, C., Tosi, G., De Filippo, D., & Verani, G. (1974). Group IIB metal complexes with thiazolidine-2-selenone and thiazolidine-2-one as ligands. *Journal of Inorganic and Nuclear Chemistry*, *36*(12), 3725-3729.
30. Balan, V., Mihai, C. T., Cojocaru, F. D., Uritu, C. M., Dodi, G., Botezat, D., & Gardikiotis, I. (2019). Vibrational spectroscopy fingerprinting in medicine: from molecular to clinical practice. *Materials*, *12*(18), 2884.
31. Gurumoorthy, G., Thirumaran, S., & Ciattini, S. (2016). Unusual octahedral Hg (II) dithiocarbamate: Synthesis, spectral and structural studies on Hg (II) complexes with pyrrole based dithiocarbamates and their utility for the preparation of α-and β-HgS. *Polyhedron*, *118*, 143-153.
32. Andrew, F. P., & Ajibade, P. A. (2018). Metal complexes of alkyl-aryl dithiocarbamates: Structural studies, anticancer potentials and applications as precursors for semiconductor nanocrystals. *Journal of Molecular Structure*, *1155*, 843-855.
33. Toscani, A., Heliövaara, E. K., Hena, J. B., White, A. J., Wilton-Ely, J. D. (2015). Multimetallic alkenyl complexes bearing macrocyclic dithiocarbamate ligands. *Organometallics*, *34*(2), 494-505.
34. Gumber, K., Sidhu, A., & Kocher, D. K. (2017). Synthesis of novel 1, 2, 4-triazole-DTC based metallo-phosphorous nanoformulations as larvicide against Aedes aegypti. *Int Res J Pure Appl Chem*, *14*(1), 1-12.
35. Almabhouh, F. A., Muhammad, F. I. A., Ibrahim, H., & Singh, H. (2019). Leptin: A pleitropic factor in physiology. *Journal of Clinical and Health Sciences*, *4*(2), 31-57.
36. Al-Jibori, S. A., Ulghafoor, M. A., Karadağ, A., Aydın, A., Akbaş, H., Ruiz, S. G. (2019). Synthesis, characterization and anti-tumor activity of Pd (II) complexes with 4, 5-benzo-3H-1, 2-dithiole-3-thione. Transition Metal Chemistry, 44, 575-583.
37. Aygun, A., Gülbagca, F., Ozer, L. Y., Ustaoglu, B., Altunoglu, Y. C., Baloglu, M. C., Sen, F. (2020). Biogenic platinum nanoparticles using black cumin seed and their potential usage as antimicrobial and anticancer agent. *Journal of pharmaceutical and biomedical analysis*, *179*, 112961.
38. Eris, S., Daşdelen, Z., & Sen, F. (2018). Enhanced electrocatalytic activity and stability of monodisperse Pt nanocomposites for direct methanol fuel cells. *Journal of colloid and interface science*, *513*, 767-773.
39. Nagao, H., Ichiji, M., & Hirasawa, I. (2017). Synthesis of platinum nanoparticles by reductive crystallization using polyethyleneimine. *Chemical Engineering & Technology*, *40*(7), 1242-1246.
40. Tian, N., Zhou, Z. Y., Sun, S. G., Ding, Y., & Wang, Z. L. (2007). Synthesis of tetrahexahedral platinum nanocrystals with high-index facets and high electro-oxidation activity. *science*, *316*(5825), 732-735.
41. Domínguez-Domínguez, S., Arias-Pardilla, J., Berenguer-Murcia, Á., Morallón, E., & Cazorla-Amorós, D. (2008). Electrochemical deposition of platinum nanoparticles on different carbon supports and conducting polymers. *Journal of Applied Electrochemistry*, *38*, 259-268.
42. Alshatwi, A. A., Athinarayanan, J., & Vaiyapuri Subbarayan, P. (2015). Green synthesis of platinum nanoparticles that induce cell death and G2/M-phase cell cycle arrest in human cervical cancer cells. *Journal of Materials Science: Materials in Medicine*, *26*, 1-9.